Tellus
SERIES A
DYNAMIC
METEOROLOGY
AND OCEANOGRAPHY
PUBLISHED BY THE INTERNATIONAL METEOROLOGICAL INSTITUTE IN STOCKHOLM

Tellus (2011), 63A, 87–106

TELLUS

A model of the coupled dynamics of climate, vegetation and terrestrial ecosystem biogeochemistry for regional applications

By BENJAMIN SMITH[1*], PATRICK SAMUELSSON[2], ANNA WRAMNEBY[1] and MARKKU RUMMUKAINEN[1,2], [1]*Department of Earth and Ecosystem Sciences, Lund University, Geocentrum II, SE-22362, Lund, Sweden;* [2]*Rossby Centre, Swedish Meteorological and Hydrological Institute, SE-60176, Norrköping, Sweden*

(Manuscript received 12 March 2010; in final form 21 July 2010)

ABSTRACT

Regional climate models (RCMs) primarily represent physical components of the climate system, omitting vegetation dynamics, ecosystem biogeochemistry and their associated feedbacks. To account for such feedbacks, we implemented a novel plant individual-based vegetation dynamics-ecosystem biogeochemistry scheme within the RCA3 RCM. Variations in leaf area index (LAI) of seven plant functional type (PFTs) in response to physical forcing and evolving vegetation state feed back to climate via adjustments in surface energy fluxes and surface properties. In an ERA-40-driven simulation over Europe, the model reproduces the recent past climate with comparable accuracy to the standard RCM. Large-scale patterns of LAI, net primary production and vegetation composition were comparable with observations, although winter LAI was systematically overestimated compared to satellite estimates. Analysis of the ERA-40 simulation and an A1B climate-change simulation revealed considerable covariation among dynamic variables of the physical climate and vegetation. At a Mediterranean site, periodic soil water limitation led to fluctuations in leaf cover and a likely positive feedback to near-surface temperature. At an alpine site, rising temperatures led to forest advance onto tundra areas, reducing albedo and effecting a likely positive feedback on temperature. Climate–vegetation coupling was less pronounced but still apparent at intermediate temperate and boreal sites.

1. Introduction

The climate system, its variations and change need to be studied comprehensively, accounting for the relevant couplings, feedback and interactions. This can only be accomplished by global climate modelling. At the same time, there is a persistent gap between the rather coarse resolution of global climate models (general circulation models, GCMs) and the need for much more detailed resolution when accounting for regional and local climates. Small-scale interactions within the climate system can add non-linearly to the larger scales (e.g. Diffenbaugh et al., 2005; Seneviratne et al., 2006). Further, climate impacts research typically depends on much more detailed information than can readily be provided by global models.

Downscaling is an established technique for closing some of the gaps mentioned above. There are statistical and dynamical downscaling approaches, the latter otherwise known as regional climate modelling (RCM; Rummukainen, 2010). Akin to global climate models, RCMs allow for comprehensive studies of regional climates, including process studies as well as projections and scenarios, further providing input to climate impact studies, as well as insights into the significance of addressing unresolved scales in global models.

Coupling of the atmosphere and the ocean has been the norm in global climate modelling for quite some time. While current efforts aim to incorporate the carbon cycle, vegetation dynamics, and atmospheric chemistry as interactive components in GCMs, current RCMs tend to focus either on the physical atmosphere and land surfaces, or the oceans and sea ice. Few coupled regional models of the physical atmosphere, land surface, sea ice and ocean exist (e.g. Döscher et al., 2002; Rinke et al., 2003; Sasaki et al., 2006; Döscher et al., 2010). The experiences point to the attractiveness of coupled regional climate models, both for pursuing climate system studies, model improvements (see also Samuelsson et al., 2003) and more versatile scenarios.

Giorgi (1995) envisaged an evolution in RCMs towards addressing vegetation, ecosystem dynamics and other interactive compartments of the climate system in a coherent way,

*Corresponding author.
e-mail: ben.smith.lu@gmail.com
DOI: 10.1111/j.1600-0870.2010.00477.x

accounting for the major feedbacks to the physical climate. At this point in time, however, the majority of RCMs focus on the physical compartments of the climate system, representing only the fast biophysical processes involved in surface-atmosphere exchange (Rummukainen, 2010).

The imperative of accounting for vegetation-based feedbacks in climate simulations was a major argument for the development of Dynamic Global Vegetation Models (DGVMs), which emerged during the late 1990s (Cramer et al., 2001). Vegetation dynamics and carbon biogeochemistry components from these models have been coupled into a number of global climate models, sometimes termed Earth system models (ESMs, e.g. Cox et al., 2000; Friedlingstein et al., 2003; Brovkin et al., 2006).

In this study, we have developed and tested a regional 'Earth' system model designed to simulate the coupled dynamics of climate and terrestrial vegetation, accounting for the major biophysical feedback mechanisms coupling the atmosphere to the land surface at regional scale and resolution. A basic research issue herein is, of course, whether feedback between the physical atmosphere and interactive vegetation does matter and, if so, which the involved mechanisms are. The model is based on state-of-the-art regional climate and dynamic vegetation/ecosystem models. Here, we focus on the skill and behaviour of the model in simulating major features of the near-surface climate and vegetation, with Europe as a case study. The focus of our analysis is on the biophysical coupling between the land surface and the atmosphere. However, vegetation dynamics in the model are closely coupled with the simulated biogeochemical cycling of carbon and water, reflecting a corresponding coupling in real ecosystems. Consequently, the model also provides a coherent framework for assessing the relative importance of biophysical and biogeochemical feedback mechanisms in various regional contexts (Betts, 2000), an issue that will be returned to in a subsequent study.

2. Methods and materials

2.1. RCA-GUESS, a coupled regional climate–vegetation dynamics model

We implemented a novel vegetation dynamics-ecosystem biogeochemistry scheme within the land surface scheme (LSS) of a regional climate model. The scheme, hereinafter referred to as the vegetation submodel, is derived from the Lund–Potsdam–Jena General Ecosystem Simulator, LPJ-GUESS, a dynamic vegetation/ecosystem model optimized for regional applications (Smith et al., 2001; Wramneby et al., 2008). The regional climate model platform, hereinafter referred to as the physical submodel, is the Rossby Centre regional atmospheric model, RCA3 (Kjellström et al., 2005; Samuelsson et al., 2011). The coupled system is referred to as RCA-GUESS.

In RCA-GUESS, vegetation dynamics and leaf phenology, simulated by the vegetation submodel, influence climate by affecting the relative cover of forest and open land which are the two vegetated fractions, or tiles, in the LSS of RCA3. The forest is divided into needleleaved and broadleaved elements while open land includes a varying coverage of herbaceous vegetation. The vegetation dynamics include variation in the leaf area indices (LAIs, the ratio of one-sided foliar area to the ground area covered) of the respective fractions on seasonal (phenological) and interannual time scales. The relative cover of different vegetation types affects surface albedo, which is a weighted average of prescribed albedo constants for needleleaved and broadleaved trees, open land vegetation, snow and non-vegetated surfaces.

LPJ-GUESS represents vegetation as a dynamic mixture of plant functional types (PFTs; Table 1). Population dynamics (establishment and mortality) are influenced by current resource status, demography, and the life-history characteristics of each PFT (Hickler et al., 2004; Wramneby et al., 2008). Individuals

Table 1. Characteristic traits of the plant functional types (PFTs) simulated by RCA-GUESS

Trait	NE	IBS	TBS	MNE	BE	G
Min T_c for establishment (°C)[a]	–	–	18	1.7	1.7	–
Max T_c for establishment (°C)[a]	2	–	6	–	–	–
Min GDD_5 for establishment[b]	600	150	830	900	2500	–
Cumulative GDD_5 for full leaf cover[b]	–	200	150	–	–	50
Optimal temperature range for photosynthesis (°C)	10–25	10–25	15–25	15–35	15–35	10–30
Leaf phenology[c]	E	S	S	E	E	S/R
Shade tolerance	High	Low	High	Low	High	Low
Drought tolerance	Low	Low	Low	High	Low	Low

Notes: NE, needleleaved evergreen tree; IBS, shade-intolerant broadleaved summergreen tree; TBS, shade-tolerant broadleaved summergreen tree; MNE, Mediterranean needleleaved evergreen tree; BE, broadleaved evergreen tree; G, grass or herb.

[a] T_c = mean temperature (°C) of coldest month of year

[b] GDD_5 = growing degree days = $\sum(T_i - 5)$; T_i = mean temperature (°C) of julian day i.

[c] E, evergreen; S, summergreen; R, raingreen.

are represented for woody PFTs (trees and shrubs) and are identical within a cohort (age class) and patch, as described below. Growth and resource competition among woody plant individuals and a herbaceous understorey govern the initial structure and composition and transient dynamics of vegetation in each patch. The input data required are mean daily temperature, precipitation and incoming short-wave radiation, as well as atmospheric CO_2 concentration, the latter affecting plant photosynthesis and stomatal regulation through biochemical (direct) and hydrological (indirect) mechanisms (Hickler et al., 2008).

Photosynthesis, respiration, tissue turnover and carbon allocation to leaves, fine roots and stems are modelled on an individual basis for trees, or on an areal basis for herbaceous, including understorey, vegetation. Height and diameter growth are regulated by carbon allocation, conversion of sapwood to heartwood, and a set of prescribed allometric relationships for each PFT. Exogenous biomass-destroying disturbances (corresponding for example to storms, fires or forest harvest) are represented as a stochastic process, here with an expectation of $0.01\ \mathrm{yr}^{-1}$, corresponding to a local expected return interval of 100 yr, a representative value for natural vegetation (Wramneby et al., 2008). Individual trees are distinguished, but are identical within each cohort. As population processes and disturbances are modelled stochastically, stand characteristics are averaged over a number of patches, here 30 per forest tile and 0.1 ha in size, representing 'random samples' of the simulated stand of vegetation. Replicate patches were not required for the open land tile; herbaceous PFT dynamics are modelled deterministically. A detailed description of LPJ-GUESS is given by Smith et al. (2001). Formulations of plant physiology, canopy-boundary layer biophysics and ecosystem biogeochemistry are in common with the global model LPJ-DGVM (Sitch et al., 2003). The version used in this study includes improved formulations of ecosystem hydrology as described by Gerten et al. (2004).

Surface energy—sensible and latent heat—fluxes from each individual tile are area-weighted to form grid-averaged fluxes. The surface energy fluxes are influenced by the characteristics of each tile represented by their LAIs, surface roughness and stomatal conductance. The latent heat flux (Wm^{-2}), which corresponds to the energy between the land surface and the atmosphere in the process of evapotranspiration/condensation, is computed based on the following general equation

$$E = \rho L_\mathrm{e} \frac{q_\mathrm{s}(T_\mathrm{s}) - q_\mathrm{am}}{r_\mathrm{a} + r_\mathrm{s}}, \tag{1}$$

where ρ is the air density (in kg m^{-3}), L_e is the latent heat of vapourization of water/ice (in J kg^{-1}), q_s is the surface saturated specific humidity at a given surface temperature, T_s, q_am is the specific humidity of the atmosphere, r_a is the aerodynamic resistance for heat fluxes (in sm^{-1}) between the surface and the atmosphere, r_s is the surface resistance to conductance of water vapour (in sm^{-1}). For the open land tile the atmosphere is represented by the lowest atmospheric layer (at 90 m in this study). The forest tile is parameterized using a double-energy balance which means that the canopy and the forest floor are given separate energy balances and surface temperatures. Here, the atmosphere is represented by the conditions of the canopy air space (Samuelsson et al., 2011). The energy fluxes between the forest and the lowest atmospheric layer are given by flux conservation of the individual fluxes from the canopy and forest floor, respectively, also influenced by the aerodynamic resistance in between. For vegetated areas, r_s equates to the inverse of aggregate stomatal conductance, and consequently scales with LAI

$$r_\mathrm{s} = \frac{r_{s,\mathrm{min}}}{\mathrm{LAI}} F_1 {F_2}^{-1} {F_3}^{-1} {F_4}^{-1} {F_5}^{-1}, \tag{2}$$

where $r_{s,\mathrm{min}}$ is the prescribed minimum surface resistance that differs for forest and open land vegetation, F_j are scalars (0–1) representing the influence of (F_1) incoming photosynthetically active radiation (PAR), (F_2) soil–water stress, (F_3) vapour pressure deficit, (F_4) air temperature and (F_5) soil temperature on surface resistance (full details are given by Samuelsson et al., 2006). For the purposes of eq. (2), the LAI's of all tree individuals and PFTs in the forest tile are aggregated to a single value for LAI. Understorey and canopy r_s are computed as separate terms. The aerodynamic resistance terms related to the lowest atmospheric layer are affected by the surface roughness of open land and forest, respectively. The aerodynamic resistance related to the forest canopy decreases with increasing LAI ($\approx$1/LAI) while the aerodynamic resistance related to the forest floor increases with increasing LAI.

Sensible heat flux is computed for each tile in a similar manner as for latent heat flux following:

$$H = \rho c_p \frac{T_\mathrm{s} - T_\mathrm{am}}{r_\mathrm{a}}, \tag{3}$$

where c_p is the specific heat capacity of the air (in J kg^{-1} K^{-1}), $T_\mathrm{s} - T_\mathrm{am}$ is the temperature differential between the surface and the atmosphere. The aerodynamic resistance, r_a, is the same as for the latent heat flux (eq. 1).

For forested areas, the relative contributions of canopy and forest floor (bare soil or snow) with respect to radiation fluxes are scaled by foliar projective cover, FPC, estimated as a function of LAI using Beer's Law (eq. 4). The albedo inversely governs the net uptake of incoming solar radiation by the land surface.

Technically, the vegetation and physical submodels are coupled together within the innermost timing loop of the physical submodel, set to a half hour in this study. Vegetation responses to the environmental driving variables simulated by the physical submodel were computed at the end of each simulation day. Half-hourly values of air temperature (canopy air space for forest, 2 m above surface for open land), soil temperature at $z = -0.14$ m, net downward shortwave radiation and soil water content (fraction of available water holding capacity, AWC) for the upper (0–0.5 m) and lower (0.5–1.5 m) soil layers distinguished in the vegetation submodel, provided by the physical submodel, are

aggregated to a daily (for radiation, daytime) average, as input to the current day simulation by the vegetation submodel. The atmospheric carbon dioxide (CO_2) concentration, required for the computation of photosynthesis and stomatal conductance, was prescribed from an external database (see Section 2.2). The vegetation model returns daily LAI estimates for needleleaved trees, broadleaved trees and understorey herbaceous vegetation in the forest tile at each gridpoint, and of vegetated parts of the open land tile, assumed to comprise herbaceous vegetation. In the case of the forest tile, LAI estimates are derived by aggregating the LAI of each of up to five simulated woody (tree/shrub) PFTs (Table 1). Fractional cover of needleleaved and broadleaved forest within the forest tile is estimated as the foliar projective cover (FPC) using Beer's law

$$\begin{aligned} A &= 2.0 - \exp(-0.5 \times \mathrm{LAI}_{\mathrm{needle}}) - \exp(-0.5 \times \mathrm{LAI}_{\mathrm{broad}}) \\ A_{\mathrm{needle}} &= [1.0 - \exp(-0.5 \times \mathrm{LAI}_{\mathrm{needle}})]/A \\ A_{\mathrm{broad}} &= [1.0 - \exp(-0.5 \times \mathrm{LAI}_{\mathrm{broad}})]/A, \end{aligned} \quad (4)$$

where $\mathrm{LAI}_{\mathrm{needle}}$ and $\mathrm{LAI}_{\mathrm{broad}}$ are the aggregate LAI's of needleleaved and broadleaved trees, respectively, within the forest tile. The vegetated fraction of the open land tile is estimated in a similar way

$$A_{\mathrm{herb}} = 1.0 - \exp(-0.5 \cdot \mathrm{LAI}_{\mathrm{herb}}), \quad (5)$$

where $\mathrm{LAI}_{\mathrm{herb}}$ is the LAI of the simulated C_3 herb (typically representing an agricultural crop such as wheat) in the open land tile. The herbaceous understorey simulated in the forest tile is assumed to be covered by trees and does not contribute to the estimation of open vegetation cover.

The relative coverage of the forest and land tiles (including vegetation-free fractions) was prescribed from the ECOCLIMAP physiographic database (Masson et al., 2003), representing present-day vegetation cover due both to natural (biogeographic) factors and human land use. Each tile was initialized with vegetation simulated by the vegetation submodel in a 'spin up' procedure beginning from a state of 'bare ground' and culminating in vegetation with a PFT composition and structure in an approximate steady state with the local climate. The spin up procedure is explained more fully in Section 2.2.1 Both trees and grasses (i.e. all PFTs in Table 1) were permitted to grow in the forest tile, while trees were excluded from the open land tile. By default, areas classes as natural vegetation in ECOCLIMAP were credited to the forest tile. However, the tile sizes were permitted to adjust dynamically from their prescribed values in the event that the simulated maximum growing season LAI summed across tree PFTs in the forest tile fell below 1, signifying marginal or stunted woody plant growth. Such adjustment could occur in any year of the simulation and could arise, for example, in areas or during periods in which annual growth was suppressed by extreme cold (alpine areas) or drought (dry climate ecosystems of the Mediterranean and northern Africa). In this event, the LAI of the simulated trees (taken to represent shrubland- or tundra-like vegetation) was transferred to the open land tile whose vegetation cover was recomputed following eq. (5), while the forested fraction was reset to zero.

2.2. Model experiments

Two model experiments (simulations) were performed, a 'recent past climate' (RP) experiment forced by global fields of the ERA-40 reanalysis dataset (Uppala et al., 2005) corresponding to the period 1961–1990, and a transient 'climate change' (CC) experiment (1961–2100) simulating coupled changes in climate and vegetation under an A1B greenhouse gas (GHG) emissions scenario forced by boundary conditions from a global simulation with the ECHAM5 AOGCM (Roeckner et al., 2006).

Common to both experiments was a rectangular simulation domain covering Europe and part of northern Africa on a rotated latitude–longitude grid at a resolution of approximately 50 × 50 km. The eight outermost rows/columns of grid cells on all sides constitute a boundary relaxation zone and are omitted from analysis.

2.2.1. Recent past climate (RP). This experiment covered the 30-yr period 1961–1990 and was forced by lateral boundary conditions and SSTs from ERA-40. The ERA-40 data were interpolated both horizontally and vertically to the boundaries of the RCA-GUESS domain, as detailed by Kjellström et al. (2005). Six-hourly forcing fields were used, interpolated linearly to the 30-min time step of the model.

The vegetation submodel requires an initialization ('spin up') in which vegetation in an approximate steady state with the initial forcing climate is grown from 'bare ground' for each vegetated tile. As the forcing climate, generated by the physical submodel, depends on the simulated vegetation, a two-stage spinup was required, the first based on observed climate to establish a 'first guess' at the vegetation as input to the physical submodel, the second based on climate generated by the physical submodel when forced by the first-guess vegetation.

The first stage of the spin up encompassed 360 simulation years, utilizing monthly values of temperature, precipitation and cloud cover fraction for the nearest $0.5 \times 0.5^{\circ}$ grid cell from the CRU TS 2.1 global historical climate database (New et al., 2000). As the CRU data set only extends back in time to 1901, data for the first 30 yr (1901–1930), detrended in the case of temperature, were cycled repeatedly for the first 300 yr of the spin up. Atmospheric CO_2 concentrations for the period from 1901 until the first year of the coupled climate simulation were taken from the database compiled by McGuire et al. (2001) based on atmospheric and ice-core measurements. The 1901 concentration was assumed for the preceding 300 yr. From 1961 the simulation continued for a further 30 yr in coupled mode, vegetation dynamics influencing the simulated climate and vice versa. In the second stage of the spinup, a new simulation was performed forced by the 30-yr time series of climate data generated during

the 1961–1990 coupled phase of the initial simulated, cycled repeatedly over 360 yr.

The full coupled simulation continued on from the spin up, commencing in simulation year 1961.

The use of an interannually varying but trend-free climate time series to force the vegetation in the second stage of the spinup is a simplifying assumption; in reality, vegetation structure at a given point in time will reflect the transient effect of climate variability and trends on plant population dynamics, disturbance regimes and species interactions over the preceding decades.

2.2.2. Climate change (CC). Boundary conditions for this simulation of a 21st-century climate change scenario were adopted from the A1B run of the ECHAM5/MPI-OM AOGCM (Roeckner et al., 2006; Meehl et al., 2007). The A1B emissions scenario provides mid-range forcing among the suite of scenarios defined by the IPCC (Nakicenovic and Swart, 2000). The radiative forcing of the RCA-GUESS simulation was based on the equivalent CO_2 concentration, accounting for the net radiative forcing of the combined trajectories in CO_2, other greenhouse gases (CH_4, N_2O, O_3 and CFCs), and sulphate aerosols under the A1B scenario, following Table 1 in Persson et al. (2007). The photosynthesis and surface conductance computations in the vegetation submodel were, however, forced by actual CO_2 concentrations (Table II.2.1 in IPCC, 2001).

The spin up procedure for the vegetation submodel was as described for the RC experiment above. RCA-GUESS was run in coupled mode from 1961 to 2100. Results from the 'future climate' part of the simulation, 1991–2100, are analysed here.

2.3. Validation data

Output from the RP simulation was compared with observations or independent reconstructions for the following variables: near-surface air temperature, precipitation, cloudiness, LAI, vegetation net primary production (NPP) and cover type/composition. For the meteorological variables, data both from the ERA-40 reanalysis (Uppala et al., 2005) and the station-based CRU product (New et al., 2000) were compared to the model-simulated fields on a seasonal basis. LAI estimates covering the land area of the model domain were obtained from the FASIR-NDVI (Sellers et al., 1996; Los et al., 2000) product of the International Land Surface Climatology Project Initiative (ISLSCP II) data collection. These data are based on spectral reflectance measurements by the satellite-mounted Advanced Very High Resolution Radiometer (AVHRR) sensor over the period 1982–1998. NPP, the annual balance between photosynthesis and autotrophic respiration, is the currency of biomass growth and a fundamental driver of downstream ecosystem processes such as canopy phenology, intra- and interspecific competition, litter production, soil carbon and nitrogen cycling and wildfire disturbance. We compared simulated NPP from the vegetation submodel of RCA-GUESS with site-based measurements from the Ecosystem Model-Data Intercomparison (EMDI) database (Olson et al., 2001). All of the available data points that are based on direct measurements and fall within the domain of this study, 72 points, were used for the comparison. A land cover map for comparison with the simulated vegetation from RCA-GUESS was derived by aggregating classes from the 'Type 1' (IGBP) MODIS land cover product from 2001 to five classes suitable for comparison with the PFT mixtures simulated by the model (Table 2).

2.4. Analysis of model output

The biophysical properties of the land surface influence the atmosphere through a variety of mechanisms related to the reflectance, ground-masking properties of the vegetation canopy, the influence of surface roughness on surface fluxes, the effect of stomatal regulation on evapotranspiration and on the partitioning of the surface fluxes into latent and sensible components. These properties differ depending on variability in the mixture of vegetation elements (PFTs), their respective cover and LAI, and their spatial distribution in the landscape from seasonal to interannual time scales. RCA-GUESS is unique among RCMs in representing all of these factors as dynamic components on time scales longer than an annual cycle. We wished to characterize the interactions between vegetation and atmospheric dynamics in the model in different climatic (geographic) contexts and on a range of time scales, isolating the main mechanisms and their importance to the overall dynamics of the model. Because of the many factors and interactions involved, and the presence of counteracting feedbacks that can mask the contribution of individual mechanisms to the overall variability in a summary variable such as surface temperature, this is difficult to approach by the traditional pairwise intercomparison of different variables. We therefore adopted a multivariate statistical approach, factor analysis (Manly, 1994), to isolate the main dimensions of interannual variability in a suite of prognostic variables, both physical and vegetation-related, chosen to reflect the operation of different feedback mechanisms that would be expected to link the vegetation and atmospheric dynamics of the model.

We employed factor analysis based on principal component analysis (PCA, Manly, 1994). Given data for a set of n input variables, PCA yields a new set of n variables (the principal components, PCs) that are uncorrelated linear combinations of the original set organized in descending rank order of the amount of variation in the input data they represent. In many analyses, the first few PCs account for a large proportion of the overall variation and reflect the main independent factors (e.g. forcing factors, process interactions) underlying the variation in the input data. The input data are normally first standardized by subtracting the mean and dividing the result by the standard deviation. The coefficients (loadings) on each variable for each PC then range from -1 to 1 and express the standardized linear correlation between the respective variable and the PC. Interpretability can sometimes be improved by 'rotating' the original

Table 2. Aggregation of MODIS land cover data to five vegetated classes for comparison with output from RCA-GUESS. Classes from the Type 1 version (IGBP Global Vegetation Classification Scheme) of the MODIS Land Cover 2001 product were used. The land cover data were obtained from the Oak Ridge National Laboratory Distributed Active Archive Centre (ORNL-DAAC)

Aggregate class	MODIS class
Needleleaved forest	1. Evergreen needleleaf forest 3. Deciduous needleleaf forest
Broadleaved forest and savannah	2. Evergreen broadleaf forest 4. Deciduous broadleaf forest 8. Woody savannas 9. Savannas
Mixed needleleaved-broadleaved forest	5. Mixed forests
Low-stature vegetation—shrublands, grasslands and wetlands	6. Closed shrubland 7. Open shrublands 10. Grasslands 11. Permanent wetlands
Croplands or cropland-natural vegetation mosaic	12. Croplands 14. Cropland/natural vegetation mosaic
Urban and barren land	13. Urban and built-up 16. Barren or sparsely vegetated
Snow and ice	15. Snow and ice

Note: http://webmap.ornl.gov/wcsdown/wcsdown.jsp?dg_id=10004_1; page visited 19 February 2010.

PCs in their n-dimensional space. Varimax rotation (Cooley and Lohnes, 1971) attempts to maximize the contrast between the loadings for each linear combination, resulting in a new set of factors that are more clearly related to some of the input variables (loadings approaching ± 1), and less related to the others (loadings approaching 0). Rotation works better, in this respect, the fewer of the original PCs that proceed to rotation (Manly, 1994). We rotated and analysed the minimum number of factors that accounted for at least 50% of the total variation in the input variables.

We performed factor analysis, as described above, on a set of prognostic variables from RCA-GUESS whose interrelationships we expected to reveal mechanisms of vegetation-atmosphere interactions operating in different geographic and temporal contexts of our study (Table 3). For many of the variables, means for different seasons within the same year were separated as they might reflect different seasonal phenomena. As vegetation structural parameters such as LAI might exhibit a lagged response to weather prior to the current growing season, we included seasonal temperatures back to spring of the preceding year and soil water for the preceding summer as additional variables. Each data point in the resulting multivariate data set thus represents values on each of the variables in Table 3 for a given year, defined as the period from 1 December the preceding calendar year to 30 November the current year. The factor analysis employed standardized data for each of the variables in Table 3, as this is necessary to place variables with different units and ranges on a roughly equal footing when seeking covariation among them. In the case of LAI, however, it must be borne in mind that standardization will give PFTs accounting for only a minor proportion of total LAI a greater relative weight than more dominant PFTs.

Separate analyses were applied to data from four gridpoints ('focus sites'; Fig. 1), chosen to span the climate space and major vegetation zones of the study domain, from both the RP (30 yr per site) and CC (110 yr per site) experiments, the former characterizing the role of vegetation dynamics under interannually varying but 'constant average forcing' conditions [ERA-40 exhibits few overall climate trends for Europe for 1961–1990; equivalent CO_2 concentrations increase by 13% over the same period], the latter a situation in which both large-scale climate and biochemical (CO_2) forcing are changing.

Factor analysis was carried out in Version 17.0 of the SPSS Statistics software.

3. Results

3.1. Validation of Recent Past experiment

Seasonal-average predictions of surface temperature (Fig. 2), precipitation (Fig. 3) and cloudiness (Fig. 4) show reasonable overall agreement with the ERA-40 reanalysis and the CRU observational data set, the latter being the more independent comparison given that the model was forced by ERA-40 on the domain boundaries. For temperature, the model shows a general cold bias in the order of 1°C in summer, while winter

Table 3. Prognostic variables from RCA-GUESS included in factor analysis of output from the RP and CC experiments

Variable	Symbol[a]	Units[b]
Leaf area index of needleleaved trees	$LAI_{needle,s}$	$m^2\ m^{-2}$
Leaf area index of broadleaved trees	$LAI_{broad,s}$	$m^2\ m^{-2}$
Leaf area index of herbaceous vegetation	$LAI_{herb,s}$	$m^2\ m^{-2}$
Vegetated fraction (foliar projective cover) of open land tile	FPC_{opl}	–
Weighted mean shortwave albedo	α_s	–
Net shortwave radiation above canopy	Rn_s	Wm^{-2}
Surface temperature ($z = 2$ m)	T_s	°C
Surface temperature for previous year	T_{s*}	°C
Precipitation	P_s	mm mo^{-1}
Soil water content[c]	θ_s	–
Soil water content for previous summer[c]	θ_{JJA*}	–
Evaporative fraction $[E/(E + H)]$	EF_s	–
Snow cover fraction	$A_{sn,s}$	–

[a] s, season; DJF, Dec-Feb; MAM, Mar-May; JJA, Jun-Aug; SON, Sep-Nov.
[b] All except FPC_{opl} on tile-weighted land area basis.
[c] Fraction of available water-holding capacity.

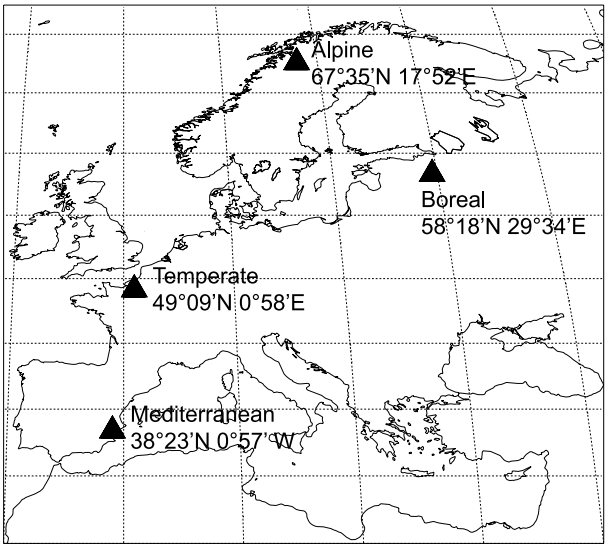

Fig. 1. Focus sites (gridpoints) selected for detailed analysis of temporal variability in simulated climate and vegetation parameters.

temperatures appear to be overestimated in the northeast of the study area and underestimated over land areas of the Mediterranean and northern Africa. Precipitation tends to be overestimated over land areas with a consistent positive bias over central and northern Europe in summer, particularly in mountain areas such as the Alps, Scandes and Scottish Highlands. Cloud cover is known as an uncertain variable in climate models and also tends to be undersampled and coarsely estimated observationally. As such, the moderate departure of the simulated cloud cover from the observational data in most parts of the study domain does not lend itself to ready interpretation. A comprehensive evaluation of cloudiness and radiation simulation by the standard version of RCA3 is available in Willén (2008).

The overall magnitude and pattern of bias in temperature and precipitation are very similar to those documented for the standard version of RCA3 that lacks dynamic vegetation (Samuelsson et al., 2011). The wintertime warm bias in the northeast of the study area may be explained by the underestimation of snow cover by the model, but may also reflect a cold bias in the measurements (Samuelsson et al., 2011). The summer cold bias is not present over central and north Europe in the standard version of RCA3. The difference in temperature bias may be connected to differences in LAI. The standard version of RCA3 has $LAI_{needle} = 4$ with LAI_{broad} in the range 0.4–4 and LAI_{herb} in the range 0.4–2.3. These LAI values are generally lower than those in RCA-GUESS (Fig. 5). Since both the aerodynamic resistance for heat fluxes for forest canopy and the surface resistance (eq. 2) become lower for higher LAI, the surface fluxes may become larger in RCA-GUESS and lead to a lower temperature.

Overestimates, relative to observations, of precipitation in mountain areas of the model domain correspond to orographic rainfall. This tends to be underestimated in the ERA-40 reanalysis due to the coarser grid resolution which results in mountain regions being smoothed out and lowered in the underlying orography database. The station-based CRU data most likely also exhibit some underestimation of rainfall in mountain areas due to undersampling by rain-gauges in periods characterized by snowfall and high winds (Frei et al., 2003). For further analysis of model performance with respect to seasonal meteorology, the reader is referred to Samuelsson et al. (2011).

RCA-GUESS simulates LAI in the ballpark of remotely sensed observations for the summer months, but appears to systematically overestimate LAI in winter, with the possible

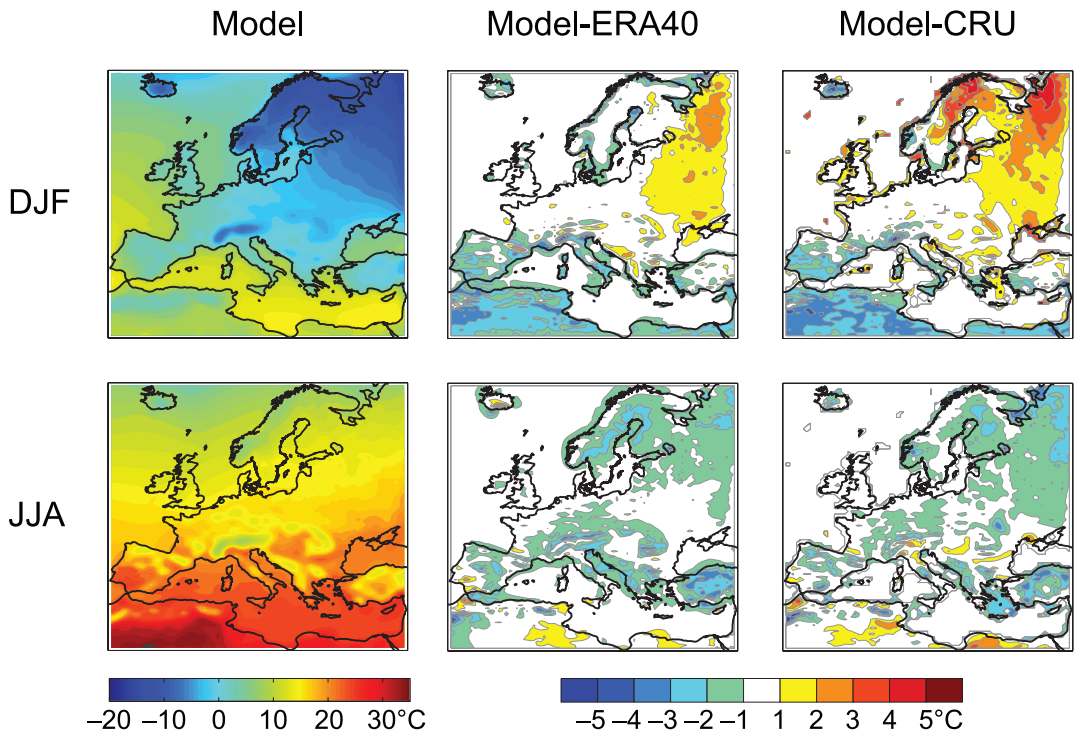

Fig. 2. Simulated ('Model') mean seasonal 2m-temperature (°C) for the ERA-40-driven Recent Past (RP) experiment, 1961–1990, and anomalies relative to the ERA-40 and CRU observational datasets. DJF = Winter (Dec-Feb); JJA = Summer (Jan-Jun).

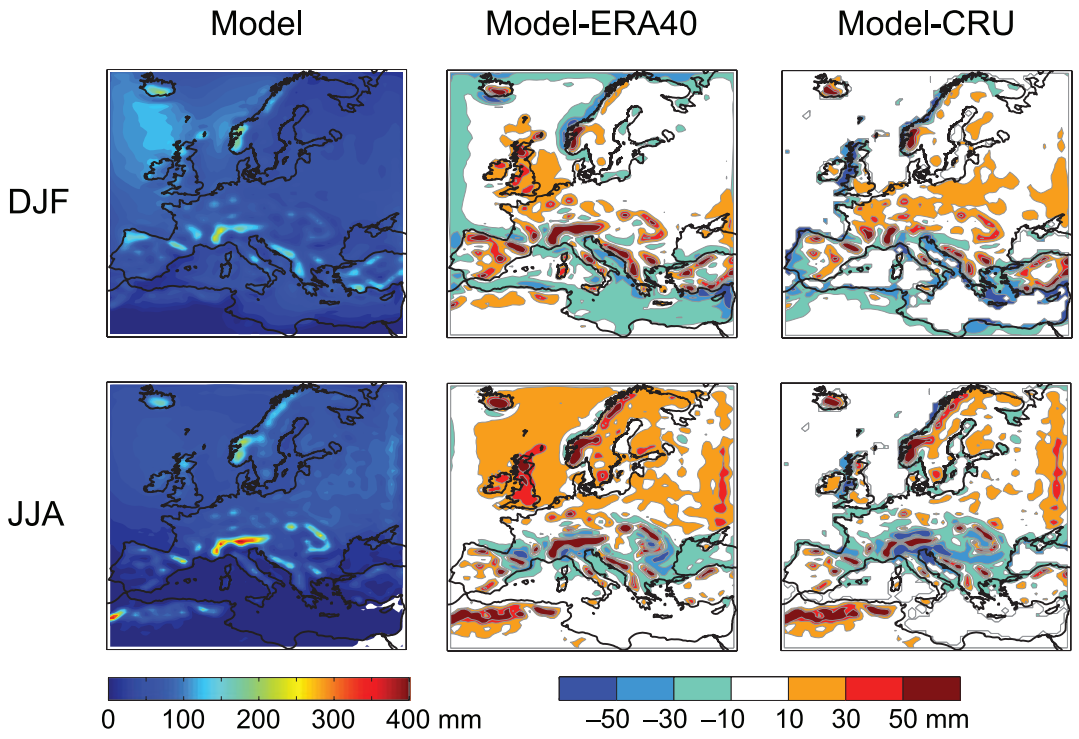

Fig. 3. Simulated total precipitation (mm over the given 3-month period) and anomalies relative to ERA-40 and CRU in the RP experiment (see Fig. 2).

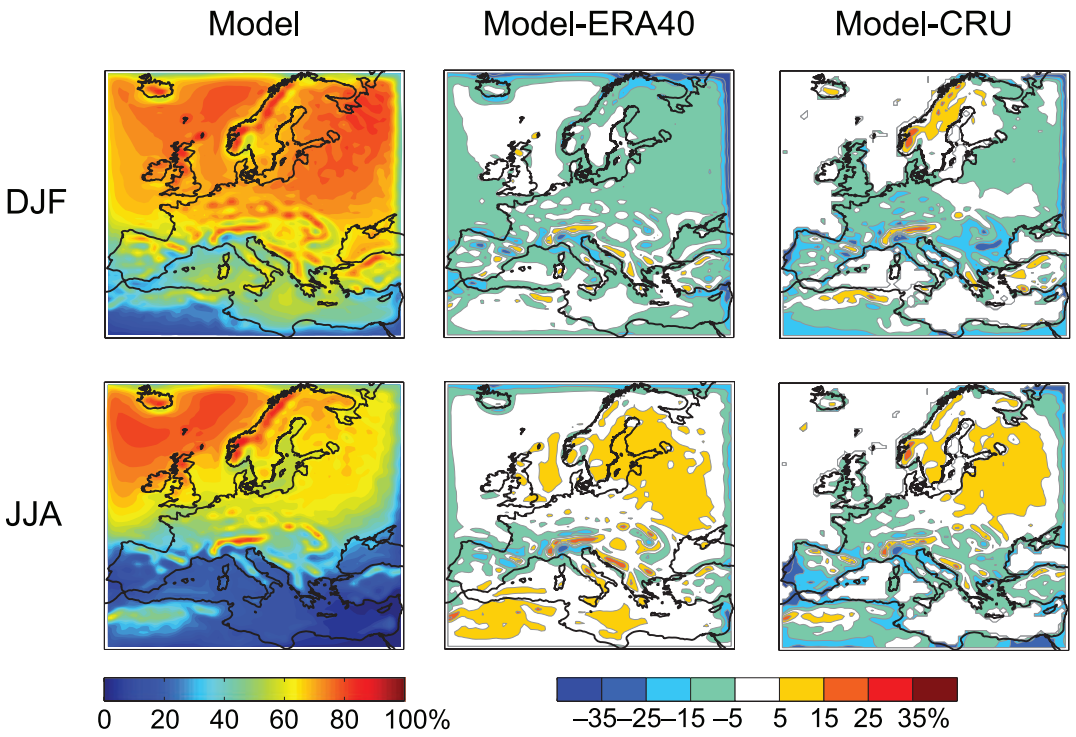

Fig. 4. Simulated cloud cover (%) and anomalies relative to ERA-40 and CRU in the RP experiment (see Fig. 2).

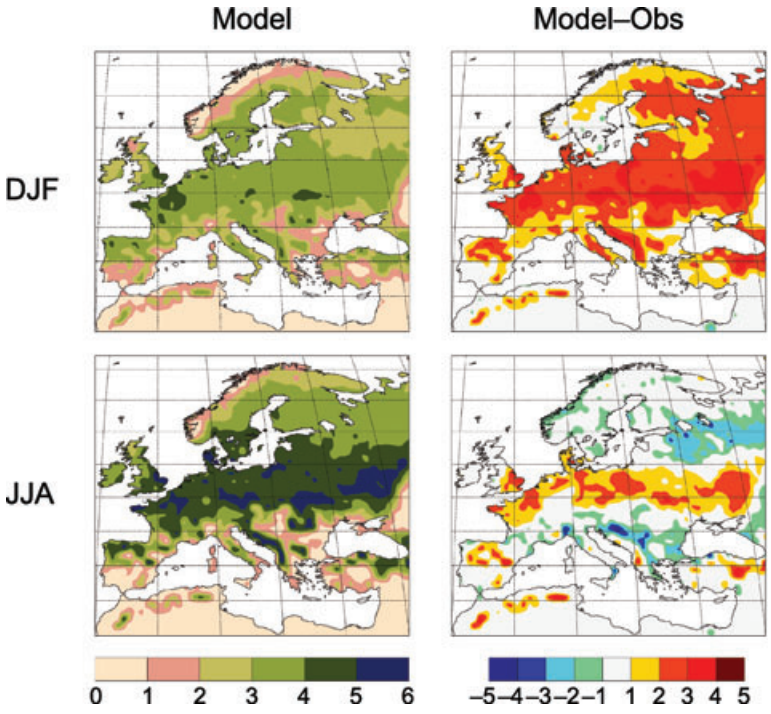

Fig. 5. Simulated seasonal tile-weighted leaf area index (mean for 1961–1990) from the RP experiment and anomalies relative to estimates from the satellite-based ISLSCP II data set (mean for 1982–1998).

exception of Scandinavia (Fig. 5). Linear regression of the model data on the satellite estimates for JJA yield a slope coefficient of 0.72 with 59% (R^2) of the spatial variation in LAI explained by the regression model. For DJF the slope is 0.94 but only 20% of the spatial variation is explained. The wintertime overestimation may be attributed to two main factors. First, the model does not explicitly represent evergreen phenology, but assumes that evergreen trees, which constitute a significant element in the

simulated vegetation of central and northern Europe, maintain their summer-maximum LAI year-round. Secondly, open-land areas are simulated as grass-covered and green for much of the winter months in western and southern Europe. These areas largely represent croplands which in reality include areas substantially bare of vegetation following autumn harvest. It should also be noted that the modelled LAI presented in Fig. 5 includes the living foliage of snow-covered vegetation (including open land vegetation) which would not be registered by the satellite data.

The most important consequence of the apparent wintertime LAI bias in the vegetation submodel may be an overestimation of the masking of snow by forest canopies, resulting in an unrealistically low albedo. For open land areas, this problem does not occur because snow automatically masks vegetation on open land in the model. However, there is no evidence of a general underestimation of winter albedo in the model, nor of the positive bias in winter temperatures this would lead to (Fig. 2). Although simulated winter temperatures generally exceed observations over parts of Fennoscandia and Russia (Fig. 2), similar bias occurs in the standard version of RCA that lacks vegetation dynamics (Samuelsson et al., 2011). The bias may be explained in part by an underestimation of snow cover in the simulations for this area (Samuelsson et al., 2011).

The model predicts NPP on the order of 0.5 kgC m^{-2} yr^{-1} over well-hydrated parts of central and northern Europe, declining to <0.2 kgC m^{-2} yr^{-1} in subarctic and alpine parts of northern Scandinavia and around 0.3 kgC m^{-2} yr^{-1} in Mediterranean-climate areas subject to summer drought (Fig. 6). The modelled values fall within a similar overall range to observations from the 72 data points of the EMDI data set (mean 0.45 kgC m^{-2} yr^{-1}) that occur within the model domain. There is, however, very limited spatial agreement between the modelled and observed data; linear regression of the EMDI values on the tile area-weighted modelled values for the nearest gridpoint yielded a slope coefficient of 0.2 ($R^2 = 0.13$; $P < 0.001$; $N = 72$).

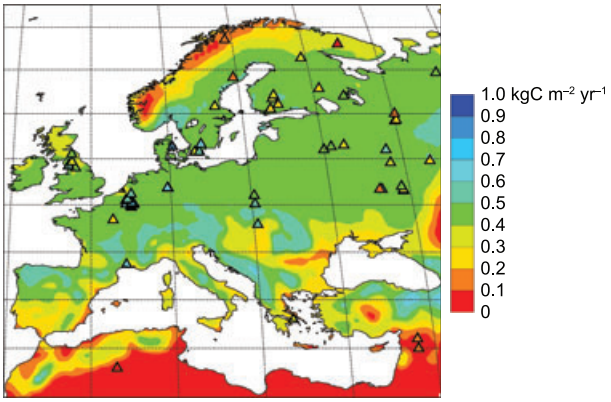

Fig. 6. Simulated tile-weighted net primary production (mean for 1961–1990) from the RP experiment compared with site-scale estimates (triangles) from the EMDI data set.

The vegetation map generated by the model under the RP experiment is shown in Fig. 7a. The map reflects the relative sizes of the forest and open land tiles at each grid point, as well as the vegetation simulated for each tile as a dynamic mixture of the PFTs defined in Table 1. In other words, the map represents a combination of actual land cover and the potential natural vegetation in dynamic equilibrium with the simulated climate (and prescribed CO_2 concentrations). Some general similarities with actual land cover (Fig. 7b) of the study area can be seen: the model appears to correctly predict the main belt of boreal needleleaved and mixed forest across Fennoscandia and eastern Russia, needleleaved forest in the Alps, low-stature vegetation (tundra) and open broadleaved woodland (mountain birch forest) in the alpine/subarctic belt of northern Scandinavia, the presence of broadleaved woodland and/or low-stature woody/herbaceous vegetation over the Iberian Peninsula and Mediterranean coastal areas. A belt of vegetation with a relatively high herbaceous fraction simulated over central and eastern Europe corresponds to cropland and cropland-natural vegetation mosaic in the MODIS data, but to the extent that the two maps coincide in this area, it is due to the relatively large open land fraction prescribed in the simulations by the ECOCLIMAP physiography database (see Methods). The simulated potential vegetation in this zone is largely broadleaved forest, which appears to have much more limited coverage over much of France, Great Britain and Ireland according to the MODIS map. However, the MODIS class 'cropland-natural vegetation mosaic class' (Table 2) may include smaller stands of both broadleaved and conifer forest.

3.2. *Analysis of Recent Past experiment*

Characteristic features of the climate and vegetation simulated at the four representative focus sites in the RP simulation are depicted in Fig. 8. For the Mediterranean focus site, the combination of cool winters with moderate rainfall and a hot, dry summer results in sparse, almost exclusively herbaceous vegetation (mean LAI <2), with a growing season confined to autumn, spring and winter (Fig. 8a). Soil water deficits in the summer months cause leaf senescence or shedding in the raingreen herbaceous PFT. Considerable interannual variability in rainfall is reflected in a likewise sizeable variation in LAI among years, reaching 4 in moister episodes of the simulation period (Fig. 9). Factor analysis confirms the tight coupling between growing season water availability and vegetation status at this site (Table 4). Two factors explain more than half of the interannual variability in the examined variables (Table 3). Factor F1 expresses the intermittent establishment of woody plants as a minor vegetation element, via a lagged response to cooler growing season temperatures the preceding year. The relationship is mediated by the effect of temperatures, via evapotranspiration, on available soil water, the most limiting resource for plant production in this seasonally harsh environment. The interannual variation in the proportion of woody plants in the vegetation is apparent

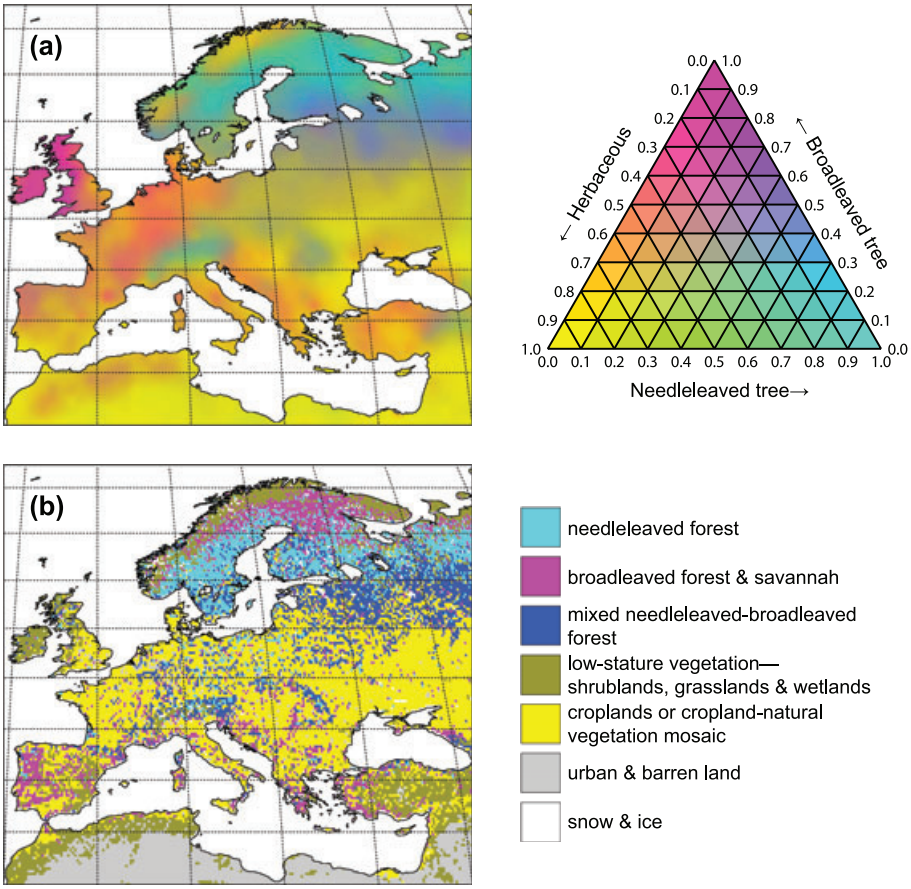

Fig. 7. (a) Average tile-weighted composition of vegetated areas in terms of fractional cover of needleleaved trees (sum of NE and MNE in Table 1), broadleaved trees (sum of TBS, IBS and BE in Table 1) and herbaceous plants (G in Table 1) simulated under the RP experiment. (b) MODIS land cover for 2001 with legend following Table 2.

in the time series of LAI depicted in Fig. 9a. Illustrative individual events for the interrelationships expressed by F1 are difficult to see in this figure, but it is apparent that woody plants (mainly comprising the broadleaved evergreen PFT) tend to be more abundant during the 1970s, coinciding with somewhat milder warmest month and annual average temperatures compared to the preceding and subsequent decades in the simulation.

The lagged vegetation response to climate may be attributed to the annual time step on which establishment and biomass growth are implemented in the vegetation submodel, new individuals entering the population on the last day of the simulation year. This feature is not unrealistic, however; recruitment is typically a lagged process in real plant communities. F2 accounts for almost as much of the total variation as F1 and primarily expresses the joint contribution of precipitation and vegetation cover/LAI, via soil water content, to the evaporative fraction (EF) of the surface–atmosphere heat flux. A negative relationship between EF and temperature in spring suggests a possible LAI-mediated feedback on temperature, as the direct effect of temperature on evapotranspiration would be the opposite, higher temperatures increasing transpirative demand. The contribution of Rn_{MAM}, as a negative term, appears to reflect the influence of cloud cover on precipitation, which appears as a positive term for the same season. The prominence of albedo within this factor may be assumed to result from the differing contributions of cover-specific albedo constants to the weighted average, bare ground having a lower prescribed constant (less reflection of incoming radiation) compared to vegetation.

The simulated climate of the temperate site (Fig. 8b) imparts favourable conditions for vegetation growth with sufficient soil water during most of the long growing season, even though a rainfall minimum occurs in summer. The resulting simulated vegetation is the most productive and luxuriant among the four focus sites, attaining an LAI of ∼5. Broadleaved trees dominate the simulated vegetation in the forest tile. In the absence of a very strong controlling influence of water availability, the interrelationships among climate and vegetation variables are weaker compared to the Mediterranean site (Table 4b). Four independent factors accommodate half of the total variation. F1 is analogous to F2 from the Mediterranean site, expressing influences of cloud cover ($-Rn$) and precipitation on soil water, and the joint effect of soil water and vegetation cover/LAI on

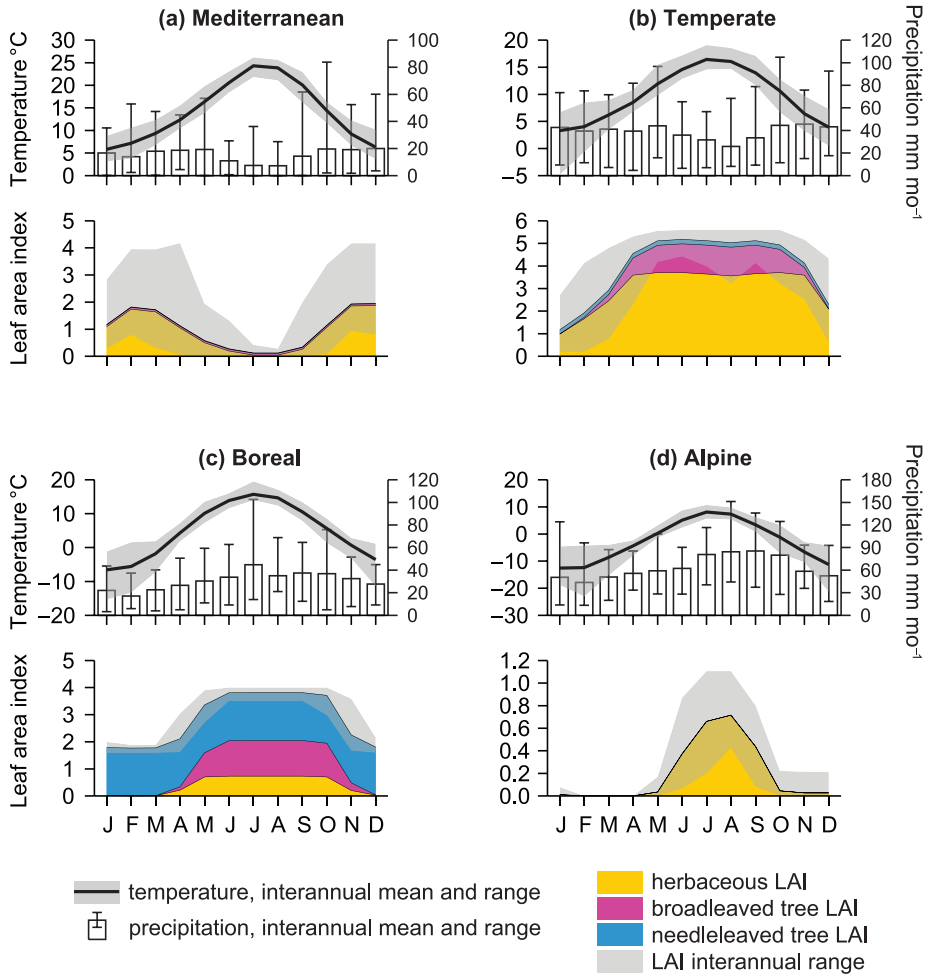

Fig. 8. Seasonal variation in simulated temperature, precipitation and leaf area index at the four focus sites (Fig. 1) in the RP experiment showing the mean and interranual range for each variable in each calendar month for the simulation period 1961–1990.

EF. A negative feedback on temperature is implied for JJA, although a relationship to the previous-years MAM temperatures cannot be explained in this way. F2 expresses the covariation in simulated LAI among, particularly, woody PFTs, reflecting interannual variation in growing conditions, which appear to influence the NPPs of different PFTs synchronously, notwithstanding the competition between them (which would tend to promote negative covariation between PFTs). F2 is only weakly correlated to physical variables such as temperature and soil water content, suggesting multifactorial responses of productivity to climate in the simulations for this area. F3 seems to suggest a tendency for later leaf onset in deciduous broadleaved forest in years with a wetter, cloudier spring. The relationship cannot be causal, as leaf onset in the vegetation model is dependent only on accumulated temperatures, not soil water. However, a strong negative relationship to temperatures the preceding summer may suggest that this factor represents a lagged dependency in the simulated climate. Just one variable, winter herbaceous LAI, has a loading >0.5 on F4. The herbaceous PFT is winter deciduous, but sheds its leaves only if mean temperatures for a 30-d period fall below a threshold temperature of 0°C. The temperate focus site occupies a transition zone in which negative temperatures occur in some, but not all, years of the simulation (Fig. 9b). This may explain a relatively significant interannual variation in winter LAI for the herbaceous PFT.

Mean temperatures simulated for the boreal focus site (Fig. 8c) range from ca. 5°C in January to ca. 15°C in the summer months. There is ample soil water throughout the growing season, with a rainfall peak in summer. The simulated vegetation of the forest tile comprises an approximately even mixture of needleleaved and broadleaved deciduous trees. Three factors were extracted. F1 represents the complementary relationship resulting from the shading of the forest understorey by the tree canopy; a denser canopy (higher tree LAI) enhances light attenuation, reducing the productivity and cover of the understorey. A positive relationship to spring insolation may be explained by the faster leaf onset (Table 1) on the part of the herbaceous PFT compared with the deciduous canopy element (TBS, IBS),

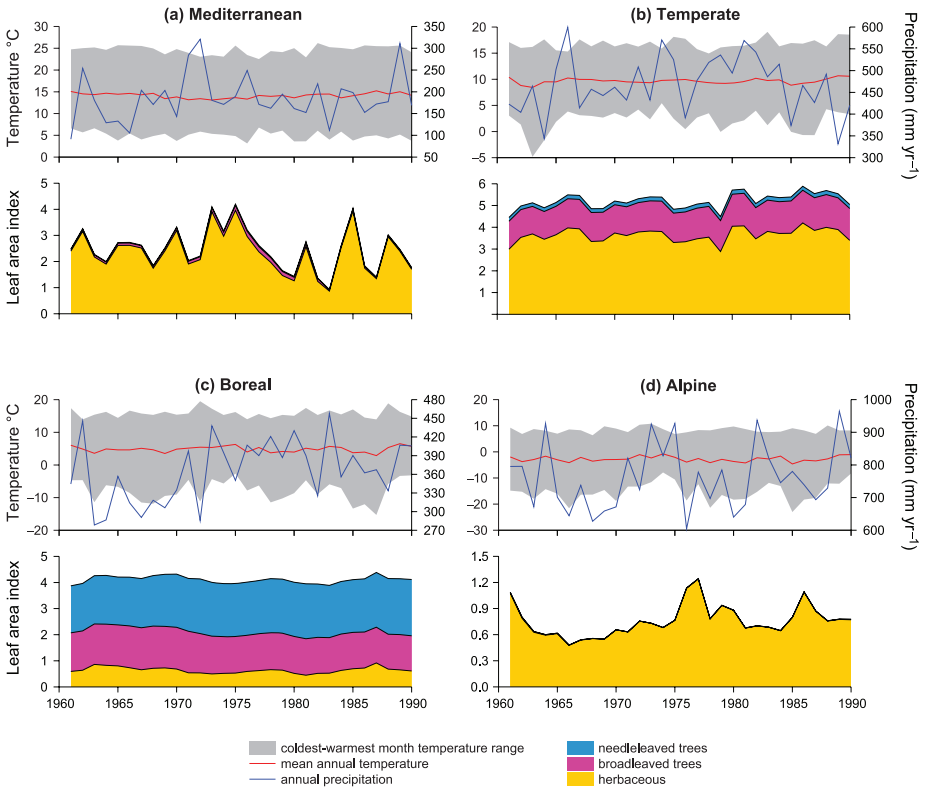

Fig. 9. Time-series of simulated temperature, precipitation and leaf area index at the four focus sites in the RP experiment, 1961–1990.

providing a growth flush in the understorey during early spring, that would benefit from cloud-free conditions (high *Rn*). The second most important factor expresses a positive relationship between summertime soil water and EF. *Rn* is a negative covariate which may reflect increased cloud formation associated with an increased load of water vapour from local or regional evapotranspiration (P_{JJA} is not a major covariate of F2, which might otherwise suggest the opposite causality). The third factor accomodates interannual variability in spring and winter temperatures with associated variables. Warmer temperatures are associated with increased precipitation. Although much of this would fall as snow, snow cover is negatively correlated to the factor, both for spring and winter, presumably reflecting faster or repeated melting in warmer years. Reduced snow cover attenuates albedo, providing a possible causal link to the milder temperatures suggested by this factor.

The Scandes mountain range in northern Scandinavia represents one of the coldest areas of the study domain as simulated by the model (Fig. 8d). Low coldest-month temperatures inhibit colonization by trees (Table 1) while a short growing season limits the productivity of the herbaceous PFT (here representing tundra vegetation in general), resulting in an LAI $\leq$1 in most years, among the lowest simulated. Four factors were extracted (Table 4d). The strongest of these is associated with winter snowfall, which tends to be greater under milder winters and seems to result in a deeper snow pack that remains into the summer months, upholding soil moisture. A positive relationship to late-season LAI is difficult to interpret mechanistically. F2 reveals that vegetation cover and leafiness are positively correlated with temperatures the preceding summer. Higher temperatures would tend to stimulate photosynthesis in this cold environment, where ambient temperatures even during the growing season are below the functional optimum (Table 1). In addition, warmer peak season temperatures are most likely associated with an earlier leaf onset and later leaf shedding—a longer growing season. Both factors will tend to increase NPP and canopy development (LAI) the following year in the model and in reality. A strong correlation with summer evapotranspiration reflects the influence of leaf cover. However, the resultant increased partitioning of the surface heat flux to latent heat is not sufficient to cool the atmosphere: T_{JJA} is positively related to the factor. The third factor expresses a straightforward positive relationship between snow cover and albedo, revealing the importance of these variables for the dynamics of the model in this climatic/physiographic context. Higher albedo is associated with reduced air temperatures in the autumn. Factor F4 reflects a relationship between growing-season cloudiness, precipitation and soil water. A positive correlation with vegetation LAI cannot be readily interpreted; water would rarely if ever limit growth in this cold environment.

Table 4. Results of factor analysis for the four focus sites (Fig. 1) in the RP experiment. Variables (see Table 3) in descending rank order of loading on factor; **bold values** = loading ≥ 0.8; variables with loadings <0.5 omitted

	(a) Mediterranean		(b) Temperate			
Factor	F1	F2	F1	F2	F3	F4
	$\mathbf{LAI_{needle,MAM}}$	$\mathbf{EF_{MAM}}$	$\mathbf{EF_{JJA}}$	$\mathbf{LAI_{needle,MAM}}$	$LAI_{broad,SON}$	$LAI_{herb,DJF}$
	$\mathbf{LAI_{needle,JJA}}$	$\boldsymbol{\alpha_{MAM}}$	$\boldsymbol{-Rn_{JJA}}$	$\mathbf{LAI_{needle,JJA}}$	$-LAI_{broad,DJF}$	
	$\mathbf{LAI_{broad,JJA}}$	$\boldsymbol{\theta_{MAM}}$	$\boldsymbol{\theta_{SON}}$	$\mathbf{LAI_{needle,SON}}$	θ_{MAM}	
	$\mathbf{LAI_{broad,MAM}}$	$\mathbf{FPC_{opl}}$	$\mathbf{LAI_{herb,JJA}}$	$\mathbf{LAI_{needle,DJF}}$	θ_{JJA*}	
	$\mathbf{LAI_{needle,DJF}}$	$\boldsymbol{\alpha_{JJA}}$	$\boldsymbol{\theta_{JJA}}$		$-T_{JJA*}$	
	$\mathbf{LAI_{broad,DJF}}$			$LAI_{broad,MAM}$	$-Rn_{MAM}$	
		$-Rn_{MAM}$	P_{JJA}	$LAI_{broad,JJA}$	$-LAI_{broad,MAM}$	
	$LAI_{herb,DJF}$	θ_{JJA}	$LAI_{herb,SON}$	$LAI_{herb,MAM}$		
	$-T_{JJA*}$	α_{SON}	FPC_{opl}	$-\alpha_{SON}$		
	$-T_{MAM*}$	EF_{JJA}	α_{JJA}			
	α_{DJF}	$LAI_{herb,MAM}$	$-T_{JJA}$			
	$-T_{SON*}$	EF_{SON}	$-T_{MAM*}$			
		P_{MAM}	θ_{MAM}			
		$-Rn_{SON}$				
		P_{DJF}				
		θ_{DJF}				
		$-T_{MAM}$				
		θ_{SON}				
Explained variation (%)	27.5	26.0	19.4	14.5	12.1	10.3

	(c) Boreal			(d) Alpine			
Factor	F1	F2	F3	F1	F2	F3	F4
	$\mathbf{-LAI_{needle,DJF}}$	$\mathbf{EF_{JJA}}$	$\boldsymbol{T_{MAM}}$	$\boldsymbol{P_{DJF}}$	$\mathbf{LAI_{herb,JJA}}$	α_{MAM}	$-Rn_{MAM}$
	$\mathbf{-LAI_{needle,MAM}}$	$\boldsymbol{\theta_{JJA}}$		$\boldsymbol{T_{DJF}}$	$\mathbf{EF_{JJA}}$	$A_{sn,MAM}$	P_{MAM}
	$\mathbf{-LAI_{needle,JJA}}$	$\boldsymbol{\theta_{SON}}$	T_{DJF}	$\mathbf{-EF_{DJF}}$		$-T_{SON}$	-$LAI_{broad,MAM}$
	$\mathbf{-LAI_{needle,SON}}$	$\boldsymbol{-Rn_{JJA}}$	$-A_{sn,MAM}$		FPC_{opl}	$-\theta_{SON}$	$LAI_{herb,MAM}$
	$\mathbf{LAI_{herb,JJA}}$		$-Rn_{DJF}$	$-Rn_{DJF}$	T_{JJA}	$A_{sn,JJA}$	$-Rn_{JJA}$
	$\mathbf{-LAI_{broad,JJA}}$	P_{DJF}	EF_{MAM}	θ_{JJA}	$LAI_{broad,JJA}$	α_{JJA}	$LAI_{herb,DJF}$
		θ_{DJF}	$-\alpha_{MAM}$	$A_{sn,JJA}$	$-EF_{SON}$	α_{DJF}	$LAI_{broad,DJF}$
	$LAI_{herb,SON}$	θ_{MAM}	P_{DJF}	$LAI_{broad,SON}$	T_{JJA*}	$-P_{SON}$	α_{MAM}
	$LAI_{herb,MAM}$	$LAI_{broad,SON}$	$LAI_{broad,MAM}$	$LAI_{herb,SON}$		Rn_{SON}	θ_{JJA}
	Rn_{MAM}	α_{JJA}	P_{MAM}				
		P_{SON}	$-A_{sn,DJF}$				
			$LAI_{herb,MAM}$				
			$-\alpha_{DJF}$				
Explained variation (%)	18.0	16.9	15.5	14.5	12.9	12.3	12.0

3.3. Analysis of Climate Change experiment

At the Mediterranean focus site, changed radiative and global forcing in the CC experiment result in a mean annual temperature trend of ca. 3.5°C over the course of the simulation (Fig. 10a). The most dramatic development in the climate is, however, a reduction in precipitation by c. 50% over the 21st century. Increased temperatures combined with reduced precipitation severely impact available soil water, resulting in a decline in the herbaceous PFT, whose LAI drops to <1 in individual years. Rainfall and LAI show some covariation from year to year, a decade of chronic drought around 2080 causing a sharp negative anomaly in the simulated vegetation. The factors extracted from the 110-year time-series (Table 5) are quite similar to the corresponding factors from the RP experiment (see above for further interpretation).

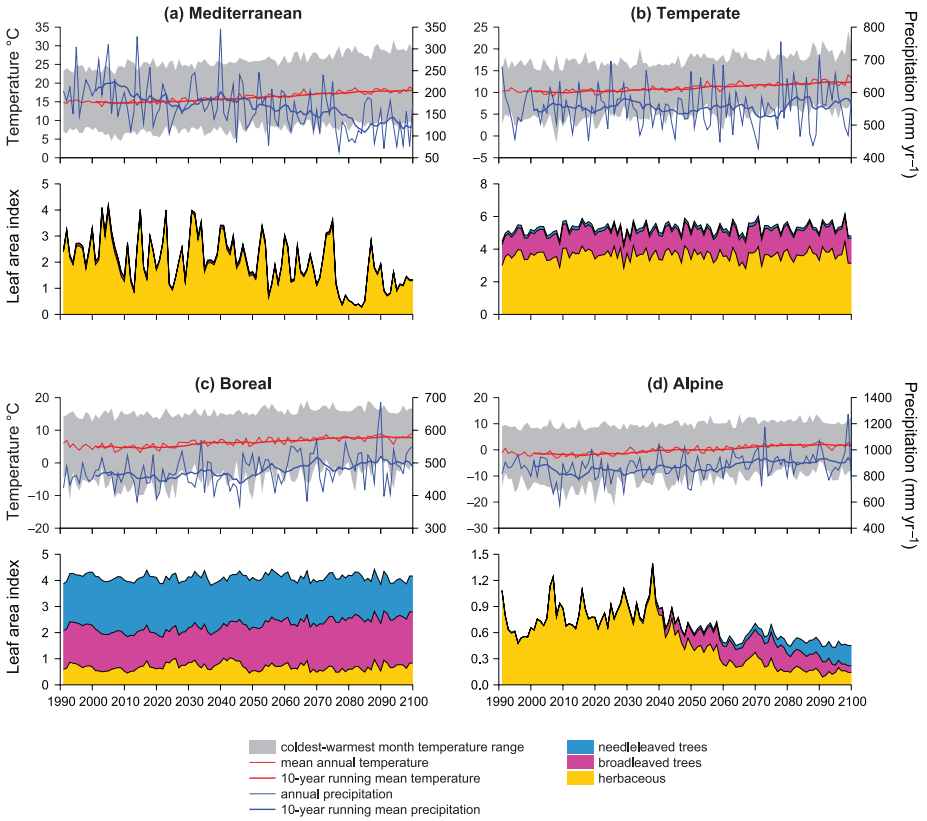

Fig. 10. Time-series of simulated temperature, precipitation and leaf area index at the four focus sites in the climate change (CC) experiment, 1991–2100.

The temperate site exhibits a warming trend in the order of 2.7°C over the course of the simulation (Fig. 10b). Precipitation exhibits considerable interannual variation but no overall trend. There is no substantial change in vegetation cover or partitioning among PFTs; however, forests (mainly broadleaved trees) increase their mean LAI on a land area basis by ca. 0.22 at the expense of the herbaceous understorey, whose LAI declines by ca. 0.13. The mechanism for this is the biochemical stimulation of photosynthesis by increased ambient CO_2 concentrations (Hickler et al., 2008); trees invest the resultant increase in their carbon reserves in an increased leaf area. This results in reduced light levels at the forest floor and a decline in understorey vegetation. A general increase in (mainly broadleaved) forest cover in this area and throughout much of central Europe is apparent for the last 30 yr of the CC experiment (Fig. 11) compared with the RP experiment (Fig. 7a). The small but steady increase in plant cover and community structure coincident with climate warming is reflected in a 'new' strongest factor F1 for the temperate site (Table 5b). Factor F2 corresponds, instead, to F1 from the RP experiment (see above) and expresses the interrelationship between cloud cover, precipitation, soil water and evaporative ratio. As previously seen, an increased partitioning of the surface energy flux to latent heat (higher EF), promoted by increased plant coverage in open land areas, appears to cool the lower atmosphere. F3 is analogous to F2 from the RP simulation, expressing the considerable interannual variation in tree LAI. Ample growing season soil water promotes increased leaf development of open land vegetation the subsequent growing season, as expressed by F4.

Mean annual temperatures at the boreal focus site increase by almost 4°C over the scenario period (Fig. 10c). Winter temperatures increase at a higher rate; the trend over the scenario period is 5.3°C. Precipitation varies considerably from year to year, but exhibits an overall positive trend, which is stronger in spring and winter than summer and autumn (results not shown). While there is no overall change in vegetation LAI, broadleaved trees increase their share of the forest canopy at the expense of needleleaved trees, in a steady trend from around 2020. The underlying cause is the steady lengthening of the growing season which shifts the competitive balance between the evergreen and deciduous habit to the advantage of deciduous trees. Increases in the broadleaved component of forest are simulated throughout an area covering much of central Europe and the transition zone into stronghold boreal forest areas in Fennoscandia and western Russia (Figs 7a and 11). Herbaceous vegetation exhibits no overall trend. The primary factor extracted by the factor analysis accounts for a full 32.7% of the overall variation in the time series (Table 5c). It expresses the negative trend, described above,

Table 5. Results of factor analysis for the four focus sites in the CC experiment. Variables in descending rank order of loading on factor; **bold** = loading ≥0.8; variables with loadings <0.5 omitted

	(a) Mediterranean		(b) Temperate			
Factor	F1	F2	F1	F2	F3	F4
	$\mathbf{LAI_{broad,MAM}}$	$\boldsymbol{\theta_{JJA}}$	$\boldsymbol{T_{DJF}}$	$\boldsymbol{\theta_{JJA}}$	$\mathbf{LAI_{needle,MAM}}$	$\mathbf{LAI_{herb,SON}}$
	$\mathbf{LAI_{broad,JJA}}$	$\mathbf{EF_{JJA}}$		$\mathbf{EF_{JJA}}$	$\mathbf{LAI_{needle,JJA}}$	
	$\mathbf{LAI_{broad,SON}}$	$\boldsymbol{\theta_{MAM}}$	$LAI_{broad,MAM}$		$\mathbf{LAI_{needle,SON}}$	$LAI_{herb,JJA}$
	$\mathbf{LAI_{needle,MAM}}$	$\mathbf{EF_{MAM}}$	$LAI_{broad,DJF}$	FPC_{opl}	$\mathbf{LAI_{needle,DJF}}$	$LAI_{herb,MAM}$
	$\mathbf{LAI_{needle,JJA}}$		$-\theta_{DJF}$	α_{JJA}		θ_{JJA*}
	$\mathbf{LAI_{needle,SON}}$	α_{MAM}	$LAI_{herb,DJF}$	θ_{MAM}		
	$\mathbf{LAI_{broad,DJF}}$	α_{JJA}	T_{SON}	$-Rn_{JJA}$		
	$\mathbf{LAI_{needle,DJF}}$	FPC_{opl}	T_{SON*}	$-Rn_{MAM}$		
		θ_{SON}	$-LAI_{broad,SON}$	θ_{SON}		
	$LAI_{herb,DJF}$	$LAI_{herb,JJA}$	T_{JJA*}	P_{MAM}		
	α_{DJF}	$LAI_{herb,MAM}$	$LAI_{broad,JJA}$	$-T_{MAM}$		
	$-T_{JJA*}$	$-Rn_{MAM}$	$-\alpha_{SON}$	$-T_{JJA}$		
	$-T_{MAM*}$	P_{MAM}	P_{DJF}	P_{JJA}		
	θ_{JJA}	EF_{SON}	T_{JJA}			
	$-T_{SON*}$	α_{SON}	EF_{MAM}			
	$-T_{DJF}$	$-T_{MAM}$				
	$-T_{JJA}$	$-T_{JJA}$				
	$LAI_{herb,MAM}$	$-Rn_{DJF}$				
		P_{DJF}				
		θ_{DJF}				
		P_{JJA}				
		$LAI_{herb,SON}$				
Explained variation (%)	26.7	26.7	17.8	15.3	10.7	7.3

	(c) Boreal			(d) Alpine			
Factor	F1	F2	F3	F1	F2	F3	F4
	$\mathbf{-LAI_{needle,MAM}}$	$-Rn_{JJA}$	$LAI_{herb,JJA}$	$\mathbf{-A_{sn,MAM}}$	$LAI_{herb,SON}$	$\boldsymbol{P_{JJA}}$	$\boldsymbol{P_{DJF}}$
	$\mathbf{-LAI_{needle,JJA}}$	θ_{JJA}	$-\theta_{DJF}$	$\mathbf{LAI_{broad,SON}}$	FPC_{opl}	$\boldsymbol{\theta_{JJA}}$	
	$\mathbf{-LAI_{needle,SON}}$	θ_{SON}	$LAI_{herb,SON}$	$\mathbf{-\alpha_{MAM}}$	$LAI_{herb,MAM}$	$\mathbf{-Rn_{JJA}}$	
	$\mathbf{-LAI_{needle,DJF}}$	EF_{JJA}	$-\theta_{MAM}$	$\mathbf{LAI_{broad,JJA}}$			
	$\boldsymbol{T_{MAM}}$	P_{JJA}	$-\theta_{JJA*}$	$\boldsymbol{T_{SON}}$			
	$\boldsymbol{\alpha_{JJA}}$			$\boldsymbol{T_{JJA}}$			
	$\boldsymbol{T_{DJF}}$			$\mathbf{-\alpha_{SON}}$			
	$\mathbf{-A_{sn,DJF}}$						
				$LAI_{needle,MAM}$			
	$LAI_{broad,JJA}$			$LAI_{needle,JJA}$			
	$LAI_{broad,MAM}$			$LAI_{needle,SON}$			
	T_{SON*}			$LAI_{needle,DJF}$			
	T_{JJA}			T_{SON*}			
	T_{SON}			$-A_{sn,SON}$			
	$-\alpha_{DJF}$			T_{MAM}			
	$-A_{sn,MAM}$			$-LAI_{herb,JJA}$			
	$LAI_{broad,SON}$			$-\alpha_{JJA}$			
	$-\alpha_{MAM}$			$-\theta_{MAM}$			
	T_{MAM*}			T_{JJA*}			
	$-Rn_{DJF}$			$-A_{sn,JJA}$			
	EF_{MAM}			T_{DJF}			
	T_{JJA*}			$LAI_{broad,MAM}$			
	$LAI_{broad,DJF}$			EF_{JJA}			
	$LAI_{broad,MAM}$			$-FPC_{opl}$			
				T_{MAM*}			
				$-A_{sn,DJF}$			
				$-Rn_{JJA}$			
Explained variation (%)	32.7	10.5	8.5	35.3	6.7	6.5	5.5

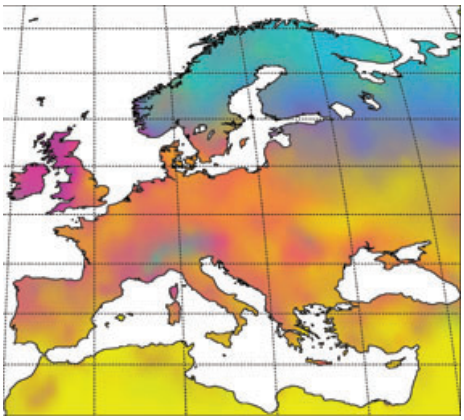

Fig. 11. (a) Average tile-weighted composition of vegetated areas in terms of fractional cover of needleleaved trees, broadleaved trees and herbaceous plants for 2071–2100 in CC experiment. Legend follows Fig. 7(a).

in the needleleaved element in favour of broadleaved trees. This coincides with warming in all seasons, reduced snow cover, and reduced albedo during the period of snow-lie. Summer albedo, by contrast, increases as a consequence of the higher albedo constant prescribed for broadleaved vegetation in the model. The second and third factors extracted explain only around 10% each of the total variation in the data, and the loadings on individual variables are varied and relatively small. F2 most strongly expresses a positive interaction between cloud cover, precipitation, soil water and evapotranspiration. The negative correlation between herbaceous vegetation cover and winter/spring soil water cannot be readily interpreted in terms of mechanisms in the model.

The alpine site shows the steepest warming trend among the four sites, mean temperatures increasing by almost 5°C and winter temperatures by ca. 6°C over the scenario period (Fig. 10d). Precipitation increases by c. 15% with the strongest trend in autumn. The influence of the warming on the simulated vegetation is considerable; broadleaved trees migrate upslope from the 2030's as their growing degree day-threshold for establishment is crossed (Table 1). Needleleaved trees appear a decade later and increase their share of the vegetation for the remainder of the simulation; by 2100, the vegetation may be characterized as subalpine woodland, reminiscent of the extant mountain birch and Scots pine-dominated woodland of mid-elevation areas in northern Fennoscandia (Tømmervik et al., 2004). The simulated displacement of tundra by boreal forest is general for alpine and subarctic areas of Scandinavia (Figs 7a and 11). Overall LAI declines; woody PFTs in the model have higher maintenance costs (inter alia for the production and repair of stems) which tends to reduce their LAI relative to herbaceous vegetation growing under similar climatic conditions (Sitch et al., 2003).

Factor analysis for the alpine site strongly reflects the simulated vegetation trends and their association with physical variables (Table 5d). The first extracted factor accommodates more than 35% of the total variation. The largest loadings are on woody vegetation LAI and temperatures for the summer and autumn months, spring and autumn snow cover (decline) and albedo (declines). Snow cover and albedo for all seasons appear as negative covariates. Increased woody plant cover, especially by evergreen needleleaved vegetation, would significantly reduce albedo during periods of snow lie. This would be expected to feed back to radiation balance and, potentially, temperatures, particularly in spring. This effect could well be expressed by F1, but appears to be compounded with a general negative relationship between snow cover and temperature.

4. Discussion

Factor analysis of the model dynamics under the RP and CC experiments reveal considerable covariation among prognostic variables reflecting the simultaneous dynamics of the physical climate and vegetation. In general, these associations are apparent in the most important (in terms of explained variability) factors of variability in the simulations, indicating an important contribution to the emergent dynamics of the model. Both explained variability and covariation among physical and vegetation-related variables are particularly pronounced at the Mediterranean and alpine sites, which from the point of view of plant physiology represent two extremes of the climate space within the simulated domain. Fluctuations and shifts in vegetation structure are correlated with interannual variability (both experiments) and decennial-scale trends (CC experiment) in driving variables of the physical climate. The key interactions are with soil water balance at the Mediterranean site and with temperature at the alpine site, highlighting the primary limiting factor for plant growth, survivorship and interspecific competition in these respective environments. The temperate and boreal focus sites are characterized by a larger degree of stability, but overall reflect a transition between the bioclimatic extremes, water playing a more important role in the temperate site and temperature at the boreal site.

Factor analysis is a correlative method and does not in itself provide any insight into causality among variables. Bearing in mind the coupling between climate and biosphere processes implemented in the model, however, at least some of the shared dynamics should reflect the operation of feedback mechanisms. Most importantly, vegetation-driven shifts in evaporative fraction affect near surface temperatures in areas and periods in which available soil water limits plant growth, leaf area and phenology. In cold-climate areas, changes in coldest-season temperatures, temperature sums (GDD) and growing season length influence the presence and density of woody vegetation, feeding back to temperature via adjustments in albedo, particularly during periods of snow lie when trees mask underlying snow.

Over the last decade, the first-generation of ESMs have proven their value in refining hypotheses about the character, potential

magnitude and geographic scope of feedbacks of land surface changes on the global climate (Chase et al., 1996; Cox et al., 2000; Betts et al., 2004; Brovkin et al., 2006; Friedlingstein et al., 2006). The results from different models, however, diverge (Friedlingstein et al., 2006), and at least some of the differences can be traced to different parametrizations of vegetation and ecosystem biogeochemical processes (Friedlingstein et al., 2003, 2006; Jones et al., 2003; Notaro et al., 2007). Most current DGVMs—and therefore the climate models to which they have been coupled—represent vegetation structure and dynamics in abstract and rather simplified ways, even compared to the available knowledge about the underlying population processes (Moorcroft, 2003; Jeltsch et al., 2008). Individual-based models of plant population and community processes have a long history and have proven robust at representing long-term dynamics of vegetation in a mechanistic and realistic way (Bugmann, 2001; Smith et al., 2001). Such models may have the potential to more accurately capture ecosystem–atmospheric coupling on interannual–centennial time scales (Moorcroft, 2003), and explicitly represent structural detail needed for the future incorporation of potentially significant feedback processes not yet considered in current ESMs; for example, methane emissions, wildfires and their emissions, and biogenic volatile organic compounds (BVOCs). Each of these phenomena may be involved in significant but as yet not fully understood interactions between atmospheric and ecosystem state (Denman et al., 2007). Their representation as interactive components in climate models will require a vegetation scheme that resolves stand structure, landscape scale heterogeneity and composition in terms of more narrowly defined PFTs (or individual taxa) than current DGVMs allow. RCA-GUESS represents a prototype of a regional Earth system model that fulfils these criteria.

As compared to an iterative coupling (Göttel et al., 2008), a fully dynamic interaction of the kind simulated by RCA-GUESS permits transient changes, lags and non-linearities in the time evolution of the climate–vegetation system to be represented in a realistic way. The differences may be significant as suggested by the simulated dynamics for the Alpine focus site; trees are established due to an increased temperature which leads to a decreased albedo, especially due to shading of snow. The establishment of trees makes the local climate even warmer which makes it even more favorable for further establishment of trees. An iterative coupling would probably show the same tendency (Göttel et al., 2008) but a fully dynamic interaction acts to enhance and accelerate the process (Cook et al., 2008).

4.1. Future perspectives

The vegetation adjustments and shifts simulated by RCA-GUESS in the CC experiment are consistent with the expected effects of the simulated climate forcing on dominant species distributions and interspecific interactions in competition for water and light. However, intercomparison studies of different DGVMs (Cramer et al., 2001) and ESMs incorporating them (Sitch et al., 2008) reveal significant differences in simulated vegetation responses to the same forcing. RCA-GUESS shares a common representation of plant physiological processes (photosynthesis, autotrophic respiration, carbon allocation) with LPJ, shown by Sitch et al. (2008) to be the only model among five DGVMs commonly coupled to AOGCMs that predicts substantial losses of needleleaved boreal forest in favour of mixed needleleaved–broadleaved forest as well as an increased cover of understorey herbs. An increase in the broadleaved deciduous component in forest was likewise simulated by RCA-GUESS in the present study. The intercomparison of different approaches to modelling vegetation dynamics, and above all attribution of differences in the behaviour of different models to the mechanisms, processes and parameters they incorporate, must be an important priority as vegetation submodels are adopted as standard components in many climate models.

RCA-GUESS is now being used to perform sensitivity experiments to identify regions and syndromes of potential vegetation-climate feedbacks under future greenhouse forcing (Wramneby et al., in press). The domain of this study spans zones of widely different climate and vegetation characteristics. Therefore, it is likely that the response in vegetation to climate change will differ between regions. Also, due to the sharp seasonality in European climates, feedback mechanisms may differ in importance both by region and season. In addition to trends in means, climate variability is likely to change in conjunction with future greenhouse forcing (Fischer and Schär, 2009); recent studies suggest that land surface-atmosphere interactions influence the magnitude of such changes (e.g. Seneviratne et al., 2006). RCA-GUESS provides a means to simulate changes in variability but, uniquely, also to infer the influence of vegetation-driven changes in land–atmosphere interactions on climate variability.

Results with RCA-GUESS (Wramneby et al., in press) show that an interactive vegetation can lead to both negative and positive feedback mechanisms related to the water balance of ecosystems (soil moisture availability). Such changes could have impacts on river discharge dynamics and availability of water for households, irrigation and industry. Ongoing development of RCA-GUESS includes a river-routing module which will provide the possibility to study the interaction between vegetation development, irrigation demand and available river water for irrigation.

Finally, the incorporation of managed land will improve the ability of the system to account for the combined effects of land management and vegetation dynamics on regional climate changes.

5. Acknowledgments

We thank two anonymous referees for helpful input to the revision of this paper. The study was funded by the Swedish Research Council for Environment, Agricultural Sciences and

Spatial Planning. It is a contribution to the Mistra Swedish Research Programme for Climate, Impacts and Adaptation (Mistra-SWECIA) and the Lund University Strategic Research Area Modelling the Regional and Global Earth System (MERGE). The model simulations were performed on the climate computing resource Tornado funded with a grant from the Knut and Alice Wallenberg foundation and housed at the National Supercomputing Centre at Linköping University.

References

Betts, R. 2000. Offset of the potential carbon sink from boreal forestation by decreases in surface albedo. *Nature* **408**, 187–190.

Betts, R. A., Cox, P. M., Collins, M., Harris, P. P., Huntingford, C. and co-authors. 2004. The role of ecosystem-atmosphere interactions in simulated Amazonian precipitation decrease and forest dieback under global climate warming. *Theor. Appl. Climatol.* **78**, 157–175.

Brovkin, V., Claussen, M., Driesschaert, E., Fischefet, T., Kicklighter, D. and co-authors. 2006. Biogeophysical effects of historical land cover changes simulated by six Earth system models of intermediate complexity. *Clim. Dyn.* **26**, 587–600.

Bugmann, H. 2001. A review of forest gap models. *Clim. Change* **51**, 259–305.

Chase, T. N., Pielke, R. A., Kittel, T. G. F., Nemani, R. and Running, S. W. 1996. Sensitivity of a general circulation model to global changes in leaf area index. *J. Geophys. Res.* **101**, 7393–7408.

Cook, B. I., Bonan, G. B., Levis, S. and Epstein, H. E. 2008. Rapid vegetation responses and feedbacks amplify climate model response to snow cover changes. *Clim. Dyn.* **30**, 391–406.

Cooley, W. W. and Lohnes, P. R. 1971. *Multivariate Data Analysis*, Wiley, New York.

Cox, P. M., Betts, R. A., Jones, C. D., Spall, S. A. and Totterdell, I. J. 2000. Acceleration of global warming due to carbon-cycle feedbacks in a coupled climate model. *Nature* **408**, 184–187.

Cramer, W., Bondeau, A., Woodward, F. I., Prentice, I. C., Betts, R. A. and co-authors. 2001. Global response of terrestrial ecosystem structure and function to CO_2 and climate change: results from six dynamic global vegetation models. *Global Change Biol.* **7**, 357–373.

Denman, K. L., Brasseur, G., Chidthaisong, A., Ciais, P., Cox, P. M. and co-authors. 2007. Couplings between changes in the climate system and biogeochemistry. In: *Climate Change 2007: The Physical Science Basis* (eds S. Solomon, D. Qin, M. Manning, M. Marquis, K. Averyt, M. M. B. and co-editors). Cambridge University Press, Cambridge, 499–587.

Diffenbaugh, N. S., Pal, J. S., Trapp, R. J. and Giorgi, F. 2005. Fine-scale processes regulate the response of extreme events to global climate change. *Proc. Natl. Acad. Sci.* **102**, 15774–15778.

Döscher, R., Willén, U., Jones, C., Rutgersson, A., Meier, H. E. M. and co-authors. 2002. The development of the coupled regional ocean-atmosphere model RCAO. *Boreal Environ. Res.*, **7**, 183–192.

Döscher, R., Wyser, K., Meier, H. E. M., Qian, M. and Redler, R. 2010. Quantifying Arctic contributions to climate predictability in a regional coupled ocean-ice-atmosphere model. *Clim. Dyn.* **34**, 1157–1176.

Fischer, E. M. and Schär, C. 2009. Future changes in daily summer temperature variability: driving processes and role for temperature extremes. *Clim. Dyn.* **33**, 917–935.

Friedlingstein, P., Dufresne, J.-L., Cox, P. M. and Rayner, P. 2003. How positive is the feedback between climate change and the carbon cycle? *Tellus* **55B**, 692–700.

Friedlingstein, P., Cox, P., Betts, R., Bopp, L., Von Bloh, W. and co-authors. 2006. Climate-carbon cycle feedback analysis: Results from the (CMIP)-M-4 model intercomparison. *J. Climate* **19**, 3337–3353.

Frei, C., Christensen, J., Dequé, M., Jacob, D. and Vidale, P. 2003. Daily precipitation statistics in regional climate models: evaluation and intercomparison for the European Alps. *J. Geophys. Res.* **108**, 4124–4142.

Gerten, D., Schaphoff, S., Haberlandt, W., Lucht, W. and Sitch, S. 2004. Terrestrial vegetation and water balance – hydrological evaluation of a dynamic global vegetation model. *J. Hydrol.* **286**, 249–270.

Giorgi, F., 1995. Perspectives for regional earth system modelling. *Global Planet. Change* **10**, 23–42.

Göttel, H., Alexander, J., Keup-Thiel, E., Rechid, D., Hagemann, S. and co-authors. 2008. Influence of changed vegetations fields on regional climate simulations in the Barents Sea Region. *Clim. Change* **87**, 35–50.

Hickler, T., Smith, B., Sykes, M. T., Davis, M. B., Sugita, S. and co-authors. 2004. Using a generalized vegetation model to simulate vegetation dynamics in the western Great Lakes region, USA, under alternative disturbance regimes. *Ecology* **85**, 519–530.

Hickler, T., Smith, B., Prentice, I. C., Mjöfors, K., Miller, P. and co-authors. 2008. CO_2 fertilization in temperate forest FACE experiments not representative of boreal and tropical forests. *Global Change Biol*. **14**, 1–12.

IPCC, 2001. *Climate Change 2001. The Scientific Basis*. Contribution of working group I to the Third Assessment Report of the Intergovernmental Panel on Climate Change. Cambridge University Press, Cambridge, UK.

Jeltsch, F., Moloney, K. A., Schurr, F. M., Köchy, M. and Schwager, M. 2008. The state of plant population modelling in light of environmental change. *Perspect. Plant Ecol. Evol. Syst.* **9**, 171–189.

Jones C. D., Cox, P. and Huntingford, C. 2003. Uncertainty in climate-carbon-cycle projections associated with the sensitivity of soil respiration to temperature. *Tellus* **55B**, 642–648.

Kjellström, E., Bärring, L., Gollvik, S., Hansson, U., Jones, C. and co-authors. 2005. A 140-year simulation of European climate with the new version of the Rossby Centre regional atmospheric climate model (RCA3). *Reports Meteorol. Climatol.* **108**, SMHI, Norrköping, Sweden.

Los, S. O., Collatz, G. J., Sellers, P. J., Malmström, C. M., Pollack, N. H. and co-authors. 2000. A global 9-year biophysical land-surface data set from NOAA AVHRR data. *J. Hydrometeor*. **1**, 183–199.

Manly, B. J. F., 1994. *Multivariate Statistical Methods: A Primer*, 2nd ed. Chapman & Hall, London.

Masson, V., Champeaux, J.-L., Chauvin, F., Meriguet, C. and Lacaze, R. 2003. A global database of Land Surface Parameters at 1-km Resolution in Meteorological and Climate Models. *J. Climate* **16**, 1261–1282.

McGuire, A. D., Sitch, S., Clein, J. S., Dargaville, R., Esser, G. and co-authors. 2001. Carbon balance of the terrestrial biosphere in the twentieth century: Analyses of CO_2, climate and land use effects with four process-based ecosystem models. *Global Biogeoch. Cycl.* **15**, 183–206.

Meehl, G. A., Stocker, T. F., Collins, W. D., Friedlingstein, P., Gaye, A. T. and co-authors. 2007. Global Climate Projections. In: *Climate Change 2007: The Physical Science Basis*, eds. S. Solomon, D. Qin, M. Manning, M. Marquis, K. Averyt, M. M. B. Tignor, H. L. Miller, Jr. and Z. Chen. Cambridge University Press, Cambridge, 747–845.

Moorcroft, P. R. 2003. Recent advances in ecosystem-atmosphere interactions: an ecological perspective. *Proc. Roy. Soc. London B* **270**, 1215–1227.

Nakicenovic, N. and Swart, R. (eds) 2000. *Special Report on Emissions Scenarios: A Special Report of Working Group III of the Intergovernmental Panel on Climate change.* Cambridge University Press, Cambridge, UK.

New, M., Hulme, M. and Jones, P. D. 2000. Representing twentieth century space-time climate variability. Part 2: development of 1901-96 monthly grids of terrestrial surface climate. *J. Climate* **13**, 2217–2238.

Notaro, M., Vavrus, S. and Liu, Z. 2007. Global vegetation and climate change due to future increases in CO_2 as projected by a fully coupled model with dynamic vegetation. *J. Climate* **20**, 70–90.

Olson, R. J., Johnson, K. R., Zheng, D. L. and Scurlock, J. M. O. 2001. *Global and Regional Ecosystem Modeling: Databases of Model Drivers and Validation Measurements*. Oak Ridge National Laboratory Report ORNL/TM-2001/196. Department of Energy, Oak Ridge, Tennessee, U.S.A.

Persson, G., Bärring, L., Kjellström, E., Strandberg, G. and Rummukainen, M. 2007. Climate indices for vulnerability assessments. *Reports Meteorol. Climatol.* **111**, SMHI, Norrköping, Sweden.

Rinke, A., Gerdes, R., Dethloff, K., Kandlbinder, T., Karcher, M. and co-authors. 2003. A case study of the anomalous Arctic sea ice conditions during 1990: Insights from coupled and uncoupled regional climate model simulations. *J. Geophys. Res.* **108**, 4275.

Roeckner, E., Brokopf, R., Esch, M., Giorgetta, M., Hagemann, S. and co-authors. 2006. Sensitivity of simulated climate to horizontal and vertical resolution in the ECHAM5 atmosphere model. *J. Climate* **19**, 3771–3791.

Rummukainen, M., 2010. State-of-the-art with regional climate models. *WIRE Adv. Rev.* **1**, 82–96.

Samuelsson, P., Bringfelt, B. and Graham, L. P. 2003. The role of aerodynamic roughness for runoff and snow evaporation in land-surface schemes—comparison of uncoupled and coupled simulations. *Global Planet. Change* **38**, 93–99.

Samuelsson, P., Gollvik, S. and Ullerstig, A. 2006. The land-surface scheme of the Rossby Centre regional atmospheric climate model (RCA3). *Reports Meteorol. Climatol.* **122**, SMHI, Norrköping, Sweden.

Samuelsson, P., Jones, C., Willén, U., Gollvik, S., Hansson, U. and co-authors. 2011. The Rossby Centre Regional Climate Model RCA3: Model description and performance. *Tellus* **63A**, 4–23.

Sasaki, H., Kurihara, K., Takayabu, I., Murazaki, K., Sato, Y. and co-authors. 2006. Preliminary results from the coupled atmosphere-ocean regional climate model developed at the Meteorological Research Institute. *J. Meteor. Soc. Japan* **84**, 389–403.

Sellers, P. J., Los, S. O., Tucker, C. J., Justice, C. O., Dazlich, D. A. and co-authors. 1996. A revised land surface parameterization (SiB-2) for atmospheric GCMs. Part 2: The generation of global fields of terrestrial biophysical parameters from satellite data. *J. Climate* **9**, 706–737.

Seneviratne, S. I., Lüthi, D., Litschi, M. and Schär, C. 2006. Land-atmosphere coupling and climate change in Europe. *Nature* **443**, 205–209.

Sitch, S., Huntingford, C., Gedney, N., Levy, P. E., Lomas, M. and co-authors. 2008. Evaluation of the terrestrial carbon cycle, future plant geography and climate-carbon cycle feedbacks using five Dynamic Global Vegetation Models (DGVMs). *Global Change Biol.* **14**, 2015–2039.

Sitch, S., Smith, B., Prentice, I. C., Arneth, A., Bondeau, A. and co-authors. 2003. Evaluation of ecosystem dynamics, plant geography and terrestrial carbon cycling in the LPJ Dynamic Global Vegetation Model. *Global Change Biol.* **9**, 161–185.

Smith, B., Prentice, I. C. and Sykes, M. T. 2001. Representation of vegetation dynamics in modelling of terrestrial ecosystems: comparing two contrasting approaches within European climate space. *Global Ecol. Biogeog.* **10**, 621–637.

Tømmervik, H., Jonansen, B., Tombre, I., Thannheiser, D., Høgda, K. A. and co-authors. 2004. Vegetation changes in the nordic mountain birch forest: the influence of grazing and climate change. *Arctic Antarctic Alpine Res.* **36**, 323–332.

Uppala, S. M., Kållberg, P. W., Simmons, A. J., Andrae, U., da Costa Bechtold, V. and co-authors. 2005. The ERA-40 re-analysis. *Q. J. Roy. Meteorol. Soc.* **131**, 2961–3012.

Willén, U., 2008. Preliminary use of CM-SAF cloud and radiation products for evaluation of regional climate simulations. *Reports Meteorol. Climatol.* **131**, SMHI, Norrköping, Sweden.

Wramneby, A., Smith, B. and Samuelsson, P. Hotspots of vegetation-climate feedbacks under future greenhouse forcing in Europe. *J. Geophys. Res.*, doi:10.1029/2010JD014307.

Wramneby, A., Smith, B., Zaehle, S. and Sykes, M. T. 2008. Parameter uncertainties in the modelling of vegetation dynamics—effects on tree community structure and ecosystem functioning in European forest biomes. *Ecol. Mod.* **216**, 277–290.